Heterogeneous Catalysis Hot Paper

Deutsche Ausgabe: DOI: 10.1002/ange.201601453
Internationale Ausgabe: DOI: 10.1002/anie.201601453

Heterogeneous Catalysis for Water Oxidation by an Iridium Complex Immobilized on Bipyridine-Periodic Mesoporous Organosilica

*Xiao Liu, Yoshifumi Maegawa, Yasutomo Goto, Kenji Hara, and Shinji Inagaki**

Abstract: *Heterogenization of metal-complex catalysts for water oxidation without loss of their catalytic activity is important for the development of devices simulating photosynthesis. In this study, efficient heterogeneous iridium complexes for water oxidation were prepared using bipyridine-bridged periodic mesoporous organosilica (BPy-PMO) as a solid chelating ligand. The BPy-PMO-based iridium catalysts (Ir-BPy-PMO) were prepared by postsynthetic metalation of BPy-PMO and characterized through physicochemical analyses. The Ir-BPy-PMOs showed high catalytic activity for water oxidation. The turnover frequency (TOF) values for Ir-BPy-PMOs were one order of magnitude higher than those of conventional heterogeneous iridium catalysts. The reusability and stability of Ir-BPy-PMO were also examined, and detailed characterization was conducted using powder X-ray diffraction, nitrogen adsorption, ^{13}C DD MAS NMR spectroscopy, TEM, and XAFS methods.*

The oxidation of water to dioxygen is an important half-reaction used to gain electrons from water in artificial photosynthetic systems.[1] Significant progress has been made in the design and synthesis of homogeneous water oxidation catalysts (WOCs), including Ru, Ir, Mn, Fe, Co, Mo, and Ni complexes.[2] In particular, the iridium-based metal complexes have been studied extensively because of their relatively high catalytic activity despite their simple molecular structures.[3] For future application in devices for artificial photosynthesis, immobilization of these homogeneous WOCs onto solid supports without any loss of catalytic activity needs to be developed.

Recently, Lin and co-workers reported the preparation of heterogeneous WOCs based on metal–organic frameworks (MOFs), in which IrCp*Cl (Cp* = pentamethylcyclopentadienyl) was bonded directly to the pore surface of the MOFs containing bipyridine and phenylpyridine ligand units (Ir-BPy-MOF).[4] The MOF-based iridium complexes catalyzed water oxidation in combination with cerium (IV) ammonium nitrate (CAN) as an oxidant.[4b] The initial turnover frequency (TOF) for Ir-BPy-MOF was approximately 0.12 min^{-1} based on O_2,[4b] and was about 40 times less than that of the analogous homogeneous catalyst [IrCp*Cl(bpy)]Cl (bpy = 2,2′-bipyridine) under identical oxidation conditions (ca. 3 mM CAN).[3j] These results can be attributed mainly to lower diffusion efficiency resulting from the small pore size of the BPy-MOF support (ca. 1 nm in diameter) compared to the molecular size of CAN (ca. 1 nm). Another limitation of the MOF-based WOCs was low structural stability under high CAN concentration (> 4.5 mM), which prevented continued reuse of the catalyst.[4b]

A novel solid, periodic mesoporous organosilica (PMO) with bipyridine ligands in the framework (BPy-PMO), was synthesized by surfactant-directed polycondensation of a 100% bipyridine-silane precursor $[(iPrO)_3Si{-}C_{10}H_6N_2{-}Si(OiPr)_3]$.[5] The BPy-PMO has a unique pore-wall structure in which bipyridine ligands are densely and regularly arranged and exposed on the pore surface (Figure 1). Various metal

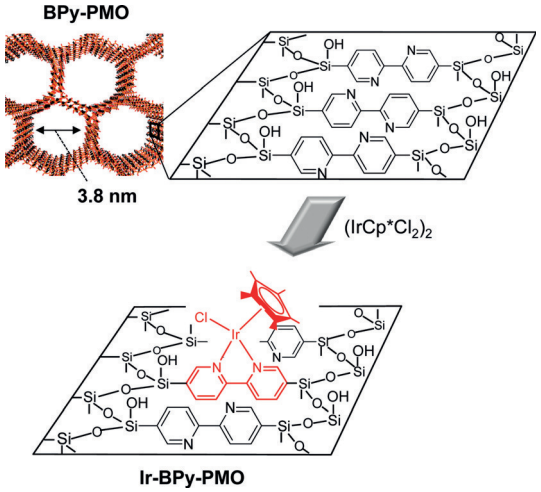

Figure 1. Schematic representations of BPy-PMO and Ir-BPy-PMO ([IrCp*Cl(BPy-PMO)]Cl).

complexes can be formed directly on the pore surface, without any linkers, by postsynthetic treatment of BPy-PMO with appropriate metal precursors. This immobilization approach is quite different from the conventional approach which involves grafting of metal complexes on the pore surface using a molecular linker. The direct formation of metal complexes on the pore surface allows smooth diffusion of substrate and product molecules in the mesochannels compared to that produced by conventional grafting using a linker. BPy-PMO also has relatively large pores with a diameter of 3.8 nm and

[*] Dr. X. Liu, Y. Maegawa, Dr. Y. Goto, Dr. S. Inagaki
Toyota Central R&D Laboratories, Inc.
Nagakute, Aichi 480-1192 (Japan)
E-mail: inagaki@mosk.tytlabs.co.jp
Prof. K. Hara
School of Engineering, Tokyo University of Technology
Hachioji, Tokyo 192-0982 (Japan)
Dr. X. Liu
Current address: Key Laboratory for Green Chemical Technology of Ministry of Education, School of Chemical Engineering and Technology, Tianjin University, Tianjin 300072 (China)

Supporting information for this article can be found under: http://dx.doi.org/10.1002/anie.201601453.

a stable covalent framework, which are advantageous for application as a solid support for heterogeneous catalysis.

The present report describes the synthesis of recyclable single-site solid catalysts, [IrCp*Cl(BPy-PMO)]Cl (Ir-BPy-PMO), and their efficient catalysis for water oxidation (Figure 1). The Ir-BPy-PMOs were synthesized successfully by postsynthetic metalation of BPy-PMO and were fully characterized using physicochemical analyses. The PMO-based WOCs showed high catalytic activity with TOF values of 2.1–2.8 min^{-1} under 3 mM CAN, and is comparable to that of the analogous homogeneous catalyst (3.0 min^{-1}) and much greater than those of conventional MOF-based and mesoporous-silica-based iridium catalysts. The Ir-BPy-PMO catalyst was recovered easily by filtration without leaching of the iridium species, and then reused for at least three runs with little loss of activity, even at high CAN concentrations of up to 15 mM.

The Ir-BPy-PMOs were prepared by postsynthetic metalation of BPy-PMO using $[IrCp^*Cl_2]_2$ as a precursor in ethanol at 78 °C (see the Supporting Information). The metalation caused a color change in the PMO powder from white to yellow, thus suggesting the formation of an iridium-bipyridine complex. The amount of iridium loaded onto the pore surface of the PMO catalyst could be controlled easily by varying the initial concentration of $[IrCp^*Cl_2]_2$, and three catalysts containing different amounts of iridium were prepared (denoted Ir_x-BPy-PMO, where x = Ir/bpy molar ratio). The Ir/bpy molar ratios were determined to be 0.03, 0.07, and 0.16 by energy-dispersive X-ray spectroscopy (EDX), and they correspond to 0.10, 0.22, and 0.51 mmol g^{-1} (Table 1; see Figure S5 in the Supporting Information). These results indicated that 5, 10, and 24% of the bpy units on the pore surface were coordinated with IrCp*Cl because the pore walls were composed of three layers of bpy units (2/3 of the bpy units were exposed on the pore surface). Measurements of X-ray diffraction patterns and nitrogen adsorption isotherms confirmed the preservation of ordered PMO structures and uniform mesoporosity of BPy-PMO even after formation of the iridium complexes (see Figures S1 and S2).

Table 1: Physical parameters and TOFs of water oxidation for BPy-PMO and Ir_x-BPy-PMO, homogeneous [IrCp*Cl(bpy)]Cl, Ir-$BPy_{1/10}$-MS, Ir-bpy-MCM-41, and Ir-BPy-MOF.

Sample	Ir loading [mmol g^{-1}]	d_{DFT}[b] [nm]	S_{BET}[c] [$m^2 g^{-1}$]	TOF[d] [min^{-1}]
BPy-PMO[a]	–	3.8	840	0
$Ir_{0.03}$-BPy-PMO	0.10	3.5	710	2.8
$Ir_{0.07}$-BPy-PMO	0.22	3.5	610	2.5
$Ir_{0.16}$-BPy-PMO	0.51	3.1	500	2.1
[IrCp*Cl(bpy)]Cl	–	–	–	3.0
Ir-bpy-MCM-41	0.37	3.2	940	0.2
Ir-$BPy_{1/10}$-MS	0.06	4.1	770	1.1
Ir-BPy-MOF[e]	0.30	≈1	–	0.12

[a] The amount of bpy in BPy-PMO was 3.18 mmol g^{-1}. [b] Density functional theory (DFT) pore diameter. [c] Brunauer–Emmett–Teller (BET) surface areas. [d] 3 mM Ce^{4+} in pH 1 HNO_3 solution with 0.5 μmol Ir. TOF was calculated per Ir atom from the data for the first 15 min. [e] Ref. [4b].

The formation of [IrCp*Cl(BPy-PMO)]Cl complexes using BPy-PMO was confirmed by ^{13}C dipolar decoupling (DD) magic-angle spinning (MAS) NMR spectroscopy and UV/vis diffuse reflectance spectrometry. The ^{13}C DD MAS NMR spectra of PMO catalysts contained new signals attributed to the Cp* ligand in the PMO catalysts (see the Supporting Information for details). The UV/vis spectrum of $Ir_{0.07}$-BPy-PMO contained a new band near $\lambda = 370$ nm in addition to the original band at approximately $\lambda = 290$ nm, caused by π–π* transition of the framework bipyridine groups (Figure 2a). The new band can be assigned to a metal-to-ligand charge transfer (MLCT) transition, which was in good accordance with the spectrum of homogeneous [IrCp*Cl-(bpy)]Cl (see Figure S8).

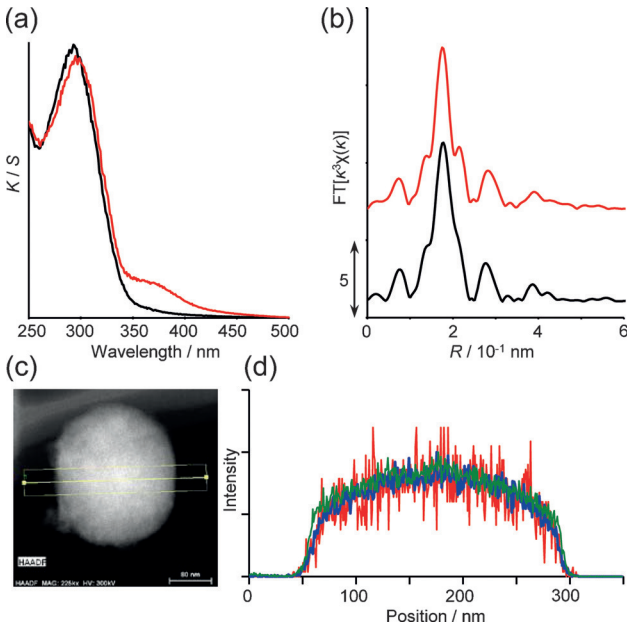

Figure 2. a) UV-vis diffuse reflectance spectra of BPy-PMO (black) and $Ir_{0.07}$-BPy-PMO (red). b) EXAFS Fourier transforms of $Ir_{0.07}$-BPy-PMO (red) and homogeneous [IrCp*Cl(bpy)]Cl (black). c,d) HAADF-STEM image and its line scan profile analysis of $Ir_{0.16}$-BPy-PMO. Red: Ir, blue: Si, green: C.

X-ray absorption fine structure (XAFS) measurements were conducted to elucidate the local structure of the iridium center in the pore walls. X-ray absorption near-edge spectroscopy (XANES) and extended X-ray absorption fine structure (EXAFS) Fourier transform at the iridium L_{III} edge showed spectral features corresponding to those of the homogeneous complex [IrCp*Cl(bpy)]Cl, thus suggesting successful formation of the desired iridium complex on the pore surface of BPy-PMO (Figure 2b; see Figures S9 and S10).

To evaluate the location of the iridium complexes in PMO, the distribution of iridium was carefully investigated. High-angle annular dark-field-scanning transmission electron microscopy (HAADF-STEM) images of $Ir_{0.16}$-BPy-PMO showed particles with a diameter of approximately 250 nm (Figure 2c). The EDX analysis revealed that the line scan profile for iridium agreed well with those for silicon and

carbon, which are the main components of BPy-PMO (Figure 2d). These results clearly show that the iridium complexes were distributed uniformly in the mesochannels of BPy-PMO.

Water oxidation reactions were conducted in the presence of the PMO catalyst and CAN as an oxidant at room temperature. Figure 3 shows time-dependent oxygen evolution curves for Ir_x-BPy-PMOs ($x = 0.03$, 0.07, and 0.16) and homogeneous [IrCp*Cl(bpy)]Cl at the same iridium and CAN concentrations (0.5 μmol Ir in 50 mL aq. HNO_3 containing 3 mM CAN). The initial TOFs, based on the amounts of O_2 produced per unit of iridium for the first 15 minutes, were 2.8, 2.5, and 2.1 min^{-1} for Ir_x-BPy-PMOs, with $x = 0.03$, 0.07, and 0.16, respectively (Table 1). Notably, the initial TOF for $Ir_{0.03}$-BPy- PMO was comparable to that for the homogeneous [IrCp*Cl(bpy)]Cl catalyst (3.0 min^{-1}), and one order of magnitude higher than that for previously reported Ir-BPy-MOF (0.12 min^{-1} based on O_2).[4b] This higher activity for Ir-BPy-PMO compared to Ir-BPy-MOF may be due to the larger pore diameter of PMO (3.5 nm) compared to that of MOF (ca. 1 nm). However, the TOF gradually decreased with an increase in the amount of the iridium complex loaded onto BPy-PMO (Table 1), which suggests that water oxidation occurred mainly in the mesochannels, because the limited diffusion should have a greater effect when more catalytic sites exist in the mesochannels. Oxygen evolution gradually leveled off as CAN was consumed, with a final O_2 yield of approximately 85%, corresponding to the limitation imposed by the amount of CAN used.

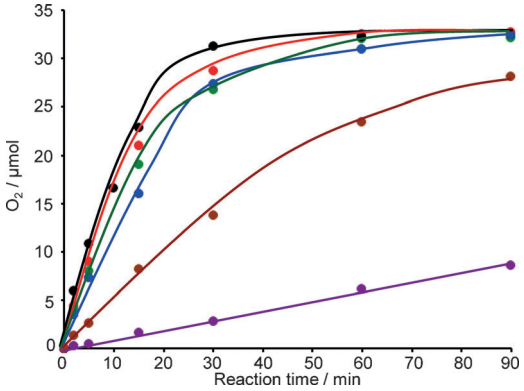

Figure 3. Time-dependent oxygen evolution curves for homogeneous [IrCp*Cl(bpy)]Cl (black), $Ir_{0.03}$-BPy-PMO (red), $Ir_{0.07}$-BPy-PMO (green), $Ir_{0.16}$-BPy-PMO (blue), Ir-$BPy_{1/10}$-MS (brown), and Ir-bpy-MCM-41 (purple). Reaction conditions: 3 mM CAN in 50 mL HNO_3 solution (pH 1) with 0.5 μmol Ir catalyst.

For comparison, the IrCp*Cl species was immobilized on different mesoporous supports, where the iridium complex was grafted on mesoporous silica (MCM-41) using a molecular linker (Ir-bpy-MCM-41) or the iridium complex was fixed directly on the surface of mesoporous silica with diluted bipyridine ligands in the silica walls (Ir-$BPy_{1/10}$-MS) (Figure 4). Interestingly, these heterogeneous iridium catalysts exhibited lower TOFs compared to Ir-BPy-PMOs, despite similar pore sizes and surface areas (Figure 3 and Table 1). The very low activity for Ir-bpy-MCM-41 was probably a result of undesirable interactions between the iridium active center and the solid surface caused by the flexible linker. Similar deactivation was reported for [Ir(cod)(OMe)(bpy)] (cod = 1,5-cyclooctadiene) grafted onto mesoporous silica (FSM-16) using a flexible linker for direct C–H borylation of benzene.[5] The lower activity of Ir-$BPy_{1/10}$-MS compared to Ir_x-BPy-PMOs suggests that the densely packed bipyridine groups on the pore surface are very important for efficient catalysis of water oxidation. Thus, BPy-PMO is a unique solid support for efficient heterogeneous iridium-catalyzed water oxidation. However, the XANES and EXAFS spectra of Ir-bpy-MCM-41 and Ir-$BPy_{1/10}$-MS were not significantly different from those of Ir-BPy-PMOs (see Figures S20–S22). Further studies are necessary to clarify the effect of the unique surface structure of BPy-PMO on the catalysis of water oxidation.

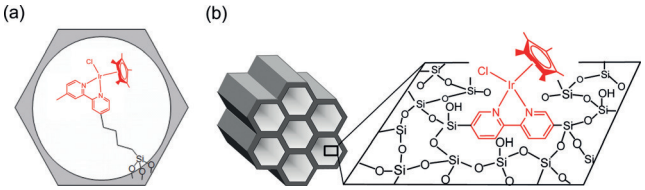

Figure 4. Schematic representations of a) Ir-bpy-MCM-41 and b) Ir-$BPy_{1/10}$-MS.

To investigate the reusability of PMO and homogeneous catalysts, water oxidation reactions were examined under repeated addition of 3 mM CAN at 20 hour intervals (Figure 5a). The $Ir_{0.07}$-BPy-PMO had nearly identical TOFs until the fourth reaction cycle. However, the homogeneous catalyst showed a gradual decrease in TOF after the first reaction cycle. This decrease may be due to catalyst deactivation caused by aggregation of the iridium complex under strong oxidizing conditions.[3d,e,f,g,i] These results suggest that BPy-PMO can effectively suppress the aggregation of the iridium complex. To check for leaching of the iridium species during the reaction, the PMO catalyst was removed by filtration after

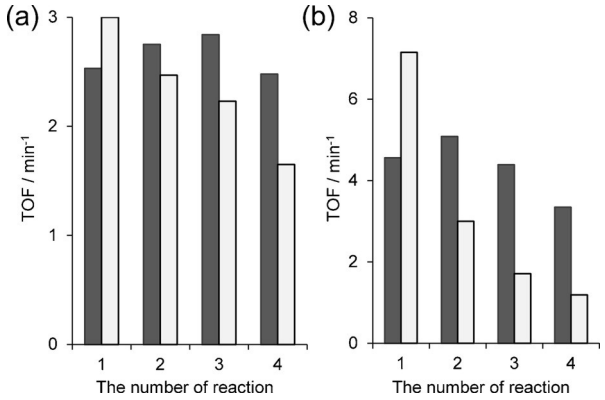

Figure 5. Changes in TOF of water oxidation for $Ir_{0.07}$-BPy-PMO (black) and homogeneous Ir catalyst [IrCp*Cl(bpy)]Cl (white) under repeated addition of CAN at CAN concentrations of a) 3 mM and b) 15 mM.

a 1 hour reaction period. No additional oxygen evolution was detected from the filtered solution (see Figure S23). Inductively coupled plasma optical emission spectroscopy (ICP-OES) of the supernatant solution showed that the iridium concentration was below the detection limit, even after the fourth reaction. These results indicate that the iridium complex coordinated strongly with the BPy-PMO support.

Next, catalytic reactions using a CAN concentration of 15 mM were performed (Figure 5b). The TOF values for both heterogeneous and homogeneous iridium catalysts increased compared to those with 3 mM CAN. However, the TOF value for Ir-BPy-PMO ($4.6\ min^{-1}$) was less than that for the homogeneous catalyst ($7.2\ min^{-1}$) for the first reaction. This result is likely due to the diffusion limitation of CAN in the mesochannels because faster diffusion is needed at higher CAN concentration. However, after the second cycle, the TOFs for the PMO catalyst were superior to those for the homogeneous catalyst. The PMO catalyst showed nearly the same TOF until the third reaction cycle, after which there was a slight decrease in the TOF. These behaviors suggest that the iridium complex is still somewhat isolated on the BPy-PMO, and enables efficient catalysis even at high CAN concentrations.

To evaluate structural changes during the reactions, the PMO catalyst was recovered by filtration and reused for the successive reactions in fresh 15 mM CAN solution. The recovered PMO catalysts were characterized by XRD, nitrogen adsorption, ^{13}C DD MAS NMR spectroscopy, high-resolution TEM, and XAFS. The XRD patterns of $Ir_{0.07}$-BPy-PMOs showed a large decrease in peak intensities for both meso- and molecular-scale periodicities during the first three reactions, thus indicating a large decrease in the structural orders of PMO (see Figure S25b). The nitrogen adsorption isotherms showed a gradual decrease in adsorption upon repeated reactions (see Figure S25a). However, the BET surface area of the PMO catalyst remained high ($436\ m^2 g^{-1}$), even after the third reaction, which enabled access of CAN and water molecules to the iridium centers located inside the channels, although structural order decreased (see Figure S24). These data explain why the PMO catalyst maintains the catalytic activity in the third reaction despite the low structural order. The BET surface area gradually decreased after the fourth reaction, which is correlated with the decrease in TOF.

The ^{13}C DD MAS NMR spectra showed a large decrease in the signals for the Cp* rings (7 and 90 ppm) owing to oxidative degradation (see Figure S26), which has been observed previously in homogeneous and MOF-based WOCs.[3e,i,4b] The signals for the bipyridine groups in the PMO framework ($\delta = 120$–160 ppm) changed very little, although a small change in their relative intensities and a new signal at $\delta = 111$ ppm were observed. These changes probably corresponded to the decomposition of the Cp* ligands. No other new signals were observed after the reaction, such as those resulting from acetic acid or formic acid generated by the oxidative degradation of the Cp* rings.[3d,e,4b]

High-resolution TEM showed the formation of nanoparticles (ca. 30 nm) on Ir-BPy-PMO after the seventh cycle (see Figure S27). These particles were cerium oxide (CeO_2), which was confirmed by EDX analysis (see Figure S28) and selected area electron diffraction (SAED) patterns (see Figure S29). The EDX analysis also showed a uniform distribution of iridium atoms on BPy-PMO, thus suggesting no formation of iridium oxide particles, even after the seventh reaction (see Figure S28). The XANES and EXAFS spectra of Ir-BPy-PMO after the seventh cycle were quite different from those of IrO_2 although they were only slightly different from those of fresh Ir-BPy-PMO (see Figures S30 and S31). The fresh $Ir_{0.07}$-BPy-PMO has only iridium(III) because the XANES spectrum coincides almost completely with that of [IrCp*Cl(bpy)]Cl (see Figure S9). After the seventh reaction, a white line at about 11215 eV increased very slightly and a weak second signal at about 11225 eV was almost retained, thus suggesting that Ir^{III} was dominant and Ir^{IV} was minor for the reused sample (see Figure S30). Junge et al. reported that a significant amount of the Ir^{IV} species (28.5–82 % IrO_2 of Ir species) was formed for homogeneous iridium catalysts after water oxidation reaction at the high CAN concentration of 170 mM.[6] Our results suggest that no iridium oxide nanoparticles form within the first seven reactions and that iridium complexes strongly coordinate with the pore surface of BPy-PMO. The slight differences in EXAFS results are due to the decomposition of the Cp* ligand and the change in the coordination environment of iridium.

In conclusion, heterogeneous WOCs with IrCp* complexes directly and uniformly fixed on the pore surface were prepared by the postsynthetic metalation of BPy-PMO. The Ir-BPy-PMO showed high catalytic activity, which was comparable to that of the analogous homogenous iridium catalyst, and was much greater than that of the conventional MOF-based iridiumm catalyst, because of the small diffusion limitation of CAN in the mesochannels. A comparison of the heterogeneous iridium catalysts prepared using different kinds of mesoporous supports (Ir-bpy-MCM-41 and Ir-$BPy_{1/10}$-MS) suggested that direct fixation of iridium complexes on the pore surface with densely packed bipyridine groups was important for efficient catalysis of water oxidation. The Ir-BPy-PMO can be reused three times without loss of activity, although large structural changes on meso- and molecular-scales were observed. These results demonstrate the potential of BPy-PMO as a solid support for efficient heterogeneous WOC and as an integration platform for the construction of artificial photosynthesis systems.

Experimental Section

Synthesis of Ir-BPy-PMO: BPy-PMO (50 mg) was added to a mixture of $[Cp^*IrCl_2]_2$ (2, 10, and 40 mg) and anhydrous EtOH (30 mL) under an Ar atmosphere. After the suspension was stirred under reflux for 24 h, the solid was filtered and washed with DMF and distilled water to remove unreacted $[Cp^*IrCl_2]_2$. The dried sample was referred to as Ir_x-BPy-PMO (x indicates the molar ratio of Ir to BPy ligand in BPy-PMO).

Ir-BPy-PMO-catalyzed water oxidation: In a typical experiment, Ir-BPy-PMO was added to a two-neck flask and evacuated for 2 h. A fresh HNO_3 solution (pH 1, 50 mL) of CAN was prepared and purged with Ar for 1 h, followed by addition of the solution to the flask through a septum (Ir: 0.5 μmol, Ce^{4+}: 3 mM). The reaction was

conducted at room temperature. A fraction of the O_2 molecules generated in the head space were quantitatively analyzed using a Shimadzu gas chromatography system (Shimadzu GC-8A) equipped with a thermal conductivity detector (TCD) and an active carbon (mesh 60/80, 3 m long) column at a specified time. The experimental error in the analysis of oxygen product was within 10%.

Acknowledgments

We wish to thank Satoru Kosaka at Toyota Central R&D Labs for the ICP-OES measurements and Dr. Tetsu Osuna at Toyota Central R&D Labs for the TEM observations. We also thank Dr. Masamichi Ikai and Dr. Takamasa Nonaka at Toyota Central R&D Labs for the XAFS measurements. We appreciate the help of Dr. Yuichiro Hayasaka at Tohoku University for obtaining the line profile analysis of EDX. The XAFS measurements were performed at SPring-8 (BL14B2: 2013B1833, 2014A1560) and BL33XU, at KEK-PF (BL12C: 2013G222), and at SAGA Light Source (BL11: 1310111SU). This work was supported by ACT-C, JST and, in part, by a Grant-in-Aid for Scientific Research on Innovative Areas "Artificial Photosynthesis" (No. 2406) from the Japan Society for the Promotion of Science (JSPS). Part of the work was supported by CINTS at Tohoku University and Nanotechnology Platform, Japan.

Keywords: heterogeneous catalysis · iridium · oxidation · supported catalysts · water chemistry

How to cite: *Angew. Chem. Int. Ed.* **2016**, *55*, 7943–7947
Angew. Chem. **2016**, *128*, 8075–8079

[1] a) C. J. Gagliardi, A. K. Vannucci, J. J. Concepcion, Z. F. Chen, T. J. Meyer, *Energy Environ. Sci.* **2012**, *5*, 7704–7717; b) Y. Zhao, J. R. Swierk, J. D. Megiatto, B. Sherman, W. J. Youngblood, D. Qin, D. M. Lentz, A. L. Moore, T. A. Moore, D. Gust, T. E. Mallouk, *Proc. Natl. Acad. Sci. USA* **2012**, *109*, 15612–15616; c) D. G. Nocera, *Acc. Chem. Res.* **2012**, *45*, 767–776.

[2] M. D. Kärkäs, O. Verho, E. V. Johnston, B. Akermark, *Chem. Rev.* **2014**, *114*, 11863–12001.

[3] a) N. D. McDaniel, F. J. Coughlin, L. L. Tinker, S. Bernhard, *J. Am. Chem. Soc.* **2008**, *130*, 210–217; b) J. F. Hull, D. Balcells, J. D. Blakemore, C. D. Incarvito, O. Eisenstein, G. W. Brudvig, R. H. Crabtree, *J. Am. Chem. Soc.* **2009**, *131*, 8730–8731; c) J. D. Blakemore, N. D. Schley, D. Balcells, J. F. Hull, G. W. Olack, C. D. Incarvito, O. Eisenstein, G. W. Brudvig, R. H. Crabtree, *J. Am. Chem. Soc.* **2010**, *132*, 16017–16029; d) D. B. Grotjahn, D. B. Brown, J. K. Martin, D. C. Marelius, M. C. Abadjian, H. N. Tran, G. Kalyuzhny, K. S. Vecchio, Z. G. Specht, S. A. Cortes-Llamas, V. Miranda-Soto, C. van Niekerk, C. E. Moore, A. L. Rheingold, *J. Am. Chem. Soc.* **2011**, *133*, 19024–19027; e) A. Savini, P. Belanzoni, G. Bellachioma, C. Zuccaccia, D. Zuccaccia, A. Macchioni, *Green Chem.* **2011**, *13*, 3360–3374; f) D. C. Hong, M. Murakami, Y. Yamada, S. Fukuzumi, *Energy Environ. Sci.* **2012**, *5*, 5708–5716; g) U. Hintermair, S. M. Hashmi, M. Elimelech, R. H. Crabtree, *J. Am. Chem. Soc.* **2012**, *134*, 9785–9795; h) A. Lewandowska-Andralojc, D. E. Polyansky, C. H. Wang, W. H. Wang, Y. Himeda, E. Fujita, *Phys. Chem. Chem. Phys.* **2014**, *16*, 11976–11987; i) R. Z. Liao, P. E. Siegbaln, *ACS Catal.* **2014**, *4*, 3937–3949; j) A. Savini, A. Bucci, G. Bellachioma, L. Rocchigiani, C. Zuccaccia, A. Llobet, A. Macchioni, *Eur. J. Inorg. Chem.* **2014**, 690–697.

[4] a) C. Wang, Z. G. Xie, K. E. deKrafft, W. B. Lin, *J. Am. Chem. Soc.* **2011**, *133*, 13445–13454; b) C. Wang, J. L. Wang, W. B. Lin, *J. Am. Chem. Soc.* **2012**, *134*, 19895–19908.

[5] M. Waki, Y. Maegawa, K. Hara, Y. Goto, S. Shirai, Y. Yamada, N. Mizoshita, T. Tani, W. J. Chun, S. Muratsugu, M. Tada, A. Fukuoka, S. Inagaki, *J. Am. Chem. Soc.* **2014**, *136*, 4003–4011.

[6] H. Junge, N. Marquet, A. Kammer, S. Denurra, M. Bauer, S. Wohlrab, F. Gärtner, M.-M. Pohl, A. Spannenberg, S. Gladiali, M. Beller, *Chem. Eur. J.* **2012**, *18*, 12749–12758.

Received: February 10, 2016
Published online: May 11, 2016

